Наносистеми, наноматеріали, нанотехнології
Nanosistemi, Nanomateriali, Nanotehnologii
2025, т. 23, № 2, сс. 523–538
https://doi.org/10.15407/nnn.23.02.0523

PACS numbers: 61.05.cp, 61.46.Df, 68.37.Hk, 78.30.Hv, 78.67.Bf, 81.07.Dc, 81.40.Ef

Synthesis and Characterization of CuO Nanoparticles: Effect of Rapid Thermal Annealing

Kenza Almi, Said Lakel, Maria Nor Elyakin Boumezrag, and Hanna Touhami

Laboratory of Metallic and Semiconducting Materials,
University of Biskra,
Biskra, Algeria

This work is a comparative study of the effect of two different annealing methods on the copper-oxide (CuO) nanoparticles' properties. These later are synthesized using the direct precipitation method. Rapid thermal annealing (RTA) and slow thermal annealing (STA) are two methods of annealing tested. The prepared samples are annealed in air at various temperatures of 300, 400, 500°C for 1 hour. Then, they are characterized by employing scanning electron microscopy (SEM), x-ray diffraction (XRD), UV–visible and Fourier Transform Infrared (FT-IR) spectroscopies. The main results revealed an increase in the grain size with both methods as the annealing temperature increases. It reaches 30.93 nm with RTA and 26.75 nm with STA at 500°C. XRD spectra show, in the case of RTA at 500°C, a significant decrease in the intense picks corresponding to the (002) and (111) orientations. This result indicates that, beyond 400°C, one hour of RTA is not suitable for enhancing CuO-nanoparticles' crystallinity compared to STA. The optical analysis demonstrates that the energy of the optical band gap in STA is higher than that in RTA. It reaches 2.88 eV at 500°C using RTA that is close to the gap value for CuO in the range of 1.8–2.8 eV. FT-IR results show, for both methods, the presence of characteristic peaks of the Cu–O bonds in the monoclinic CuO structure without any trace to Cu_2O structure. Nevertheless, samples subject to RTA for one hour are more susceptible to absorbing species of C=O bond than those subject to STA. Hence, RTA at 500°C is far from producing CuO nanoparticles with preferred characteristics. It needs further research to examine higher-temperature annealing with controlling annealing time.

Ця робота є порівняльним дослідженням впливу двох різних методів відпалювання на властивості наночастинок оксиду Купруму (CuO). Пізніше їх було синтезовано методом прямого осадження. Було протестовано два методи відпалювання: швидке термічне відпалювання (ШТВ) та повільне термічне відпалювання (ПТВ). Підготовлені зразки відпалюва-

ли на повітрі за різних температур у 300, 400, 500°C упродовж 1 години. Потім їх характеризували за допомогою сканувальної електронної мікроскопії (SEM), рентґенівської дифракції (XRD), УФ-оптичної спектроскопії та інфрачервоної спектроскопії з Фур'є-перетвором (FT-IR). Основні результати показали збільшення розміру зерен за обома методами з підвищенням температури відпалу. Він сягає 30,93 нм із ШТВ і 26,75 нм із ПТВ за 500°C. Рентґенівські дифракційні спектри показали у випадку ШТВ за 500°C значне зменшення інтенсивних піків, що відповідають орієнтаціям (002) й (111). Цей результат показав, що понад 400°C одна година ШТВ не підходить для підвищення кристалічности наночастинок CuO порівняно з ПТВ. Оптична аналіза показала, що енергія оптичної забороненої зони за ПТВ вища, ніж за ШТВ. Вона сягає 2,88 еВ за 500°C з використанням ШТВ, що близько до значення забороненої зони CuO в діяпазоні 1,8–2,8 еВ. Результати FT-IR показали для обох методів наявність характерних піків від зв'язків Cu–O у моноклінній структурі CuO без будь-яких слідів структури Cu_2O. Тим не менш, зразки, піддані ШТВ протягом однієї години, більш схильні до поглинання частинок зі зв'язками C=O, ніж зразки, піддані ПТВ. Отже, ШТВ за 500°C є далеким від утворення наночастинок CuO з бажаними характеристиками. Є потреба у подальших досліджень для вивчення відпалу за вищої температури з контролем часу відпалювання.

Key words: annealing methods, copper oxide, nanoparticles, nanoparticles' synthesis methods, rapid thermal annealing.

Ключові слова: методи відпалювання, оксид Купруму, наночастинки, методи синтези наночастинок, швидке термічне відпалювання.

(Received 24 December, 2023; in revised form, 27 December, 2023)

1. INTRODUCTION

Nanoparticles are particles of matter, whose properties are quite different from those of the corresponding bulk material [1]. Their properties depend on their size, shape, and morphology [2–4]. Thus, the main advantage of nanomaterials is that they can be used to improve current materials or create new ones having exceptional properties.

Copper oxide in its nanostructure attracts considerable attention because of its outstanding properties. It is non-toxic, its constituents are available in abundance, it is a good solar absorber [5], a good electrical conductor [6], and it is stable at high pressure and temperature [7]. The enhancement in these properties can be influenced by the morphology of its nanostructures, which in turn depends on the process of synthesis [3, 6, 8, 9].

The thermal annealing process is an important step in synthesizing nanostructures of a metal oxide including copper oxide. There

are two techniques of thermal annealing, which are slow thermal annealing (STA) and rapid thermal annealing (RTA). The influence of these kinds of annealing on the physical properties of copper oxide in the form of thin-film nanostructure is the most commonly studied by researchers [10–15]. This may be due to the diverse applications possible of this kind of nanostructure [6, 16, 17]. Some of them confirmed the efficient impact of STA in an optimum annealing-temperature range of 200–650°C on structural and electrical properties of thin copper-oxide films [10–12, 18–22], and others demonstrated that RTA is an effective and efficient technique to enhance the structural properties in a high annealing-temperature range from 400°C to 800°C for a tuning time corresponding to each temperature [13–15, 23].

Nevertheless, several studies showed the effective implementation of copper oxide in form of nanoparticle structure to produce materials for environment, energy [24–33], and therapeutics [34–38]; annealing process in operation represents an important step in synthesising copper oxide [39, 40]. There are only a few reports studied the effects of annealing temperature in the case of copper-oxide nanoparticles [24, 40, 41]. Yet, in all previous research, the annealing process was performed in different conditions, which are specific to each experimental work, and they in turn may influence the obtained results. No study was conducted so far that reported the results of the effect of the rapid and slow thermal annealing processes performed under the same experimental conditions to conclude the efficiency of one annealing method relative to the other.

Therefore, this work aims to examine the efficient effect of rapid annealing on the physical properties of copper-oxide nanoparticles compared to the slow annealing process.

2. MATERIALS AND METHODS

2.1. CuO-Nanoparticles' Synthesis

CuO nanoparticles were synthesized using the sol–gel method through the following process. 2 g of $CuSO_4 \cdot 5H_2O$ is dissolved in 20 ml of distilled water. On the other hand, 8 g of NaOH has been dissolved in 200 ml of the same solvent. Each solution is stirred separately for a few minutes at room temperature to obtain two homogenous solutions of 0.4 mol/l and 1 mol/l, respectively. Sodium hydroxide solution is completely added to the first solution of cupric sulphate and then stirred for one hour on a heating plate set at 100°C. The solution is then left to cool at room temperature; then, it is filtered to get a black powder. This later is carefully collected and dried in an oven for an hour at 100°C to evaporate all residual

solvents on the substrate surface. After that, it was milled using a ceramic mortar. Thus, copper-oxide nanoparticles are obtained.

2.2. Specimen Preparation

After synthesizing CuO nanoparticles, they were divided into two portions. From the first portion, three fractions were prepared to undergo a rapid heat annealing at 300°C, 400°C, and 500°C for one hour. In the same way, three other fractions were prepared from the second portion, but this time to undergo a slow heat annealing at the same temperatures and during the same time. In both annealing processes, a Nabertherm GmbH annealing furnace was used. It is an electrically heated furnace that heats from 30 to 3000°C.

In STA, the sample is heated gradually in the oven from room temperature to the target temperature with a heating rate of 2°C per minute. Once the set temperature is reached, heating maintains it constant for one hour; then, it automatically stops heating allowing gradual cooling of the sample. Whereas in the case of the RTA, the sample is heated directly at the desired temperature for one hour; then, it is immediately removed from the oven and cooled at room temperature. To do so, the sample is put in a special glass tube, which is brought in through a hole drilled in the back of the oven made to evacuate the vapour produced during heating.

After heat treatment, different specimens were subdivided into small amounts to be characterized.

2.3. Specimen Characterization

To determine the nanoparticles' size and shape, a morphological study was conducted using a scanning electron microscope of TESCAN-VEG03 type. Magnification of 5 μm has been used. Structural properties were studied using Rigaku Mini Flax 600 x-ray diffractometer (CuK_α radiation, $\lambda = 1.54056$ Å); x-ray diffraction patterns were set between $2\theta = 20°$ and 80° with a step of 0.5° per minute. In this intention, infrared spectrophotometry (FT-IR-8400S) was used as well. Optical properties were analyzed employing a UV–visible spectrophotometer (Perkin Elmer-Lambda 25); the spectral range was measured between 200 and 800 nm.

3. RESULTS AND DISCUSSION

3.1. Morphological Analysis

SEM images of the surface morphology of the prepared CuO

nanoparticles are presented in Fig. 1. They show that most CuO nanoparticles have a sheet-like shape. The same result was found in the literature using the same synthesizing method [41]. Actually, sheet average particle size varies in a broad range in this structure; so, it is not practical for easy to measure the particle size of our samples. Nevertheless, SEM results reveal some distinctions between the morphology of the RTA and STA samples annealed at different temperatures. RTA images at different temperatures show an inhomogeneous distribution of the nanoparticles with large conglomerates compared to STA samples [10]. This could be justified by the grain growth mechanism correlated to rapid thermal annealing [42, 43]. The fast ramping to the target temperature triggers the nucleation process within the short time; a higher temperature generates high pressure, which promotes the mutual diffusion of small and intermediate grains during annealing, resulting in larger agglomerates [10, 44].

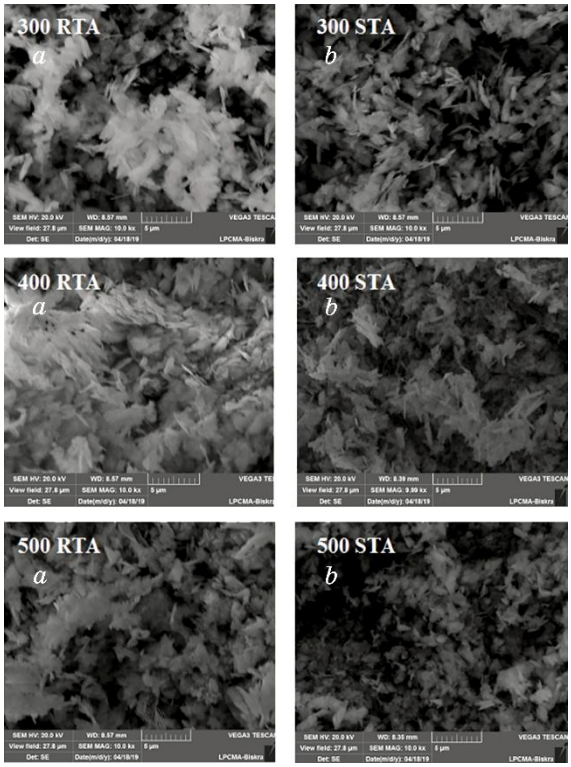

Fig. 1. SEM images of the CuO nanoparticles synthesized using (*a*) RTA and (*b*) STA at 300°C, 400°C, and 500°C for one hour of annealing.

3.2. Structural Analysis

The x-ray diffractograms of the prepared CuO nanoparticles are presented in Fig. 2. The results show that the peaks in all obtained XRD spectra are well matched with the monoclinic phase of CuO crystals (JCPDS card No. 080-1268). All samples exhibit the same preferential orientations, (111) and (002), which agree with research on copper-oxide nanoparticles [8, 9]. X-ray diffractograms' analysis demonstrates that, in both methods, the diffracted intensity of the most intense peaks increases with the increase of the temperature except for the case of RTA at 500°C, where it decreases significantly as depicted in Fig. 3, *a*, *b*. It is also noticeable that STA peaks are more intense than RTA peaks at all positions and almost at all the studied annealing temperatures (Fig. 2).

Further, Table 1 indicates that the crystallite size calculated in both techniques of annealing increases with the increase of the temperature, but it takes higher values in RTA cases.

To explain those observations, it is necessary to return to the factors associated with both peak intensity and crystallite size. Thermal treatment increases the crystalline nature, which leads to an increase in the number of grains orientated in a particular direction. By increasing the annealing temperature, many different grains of the same orientation coalesce together and form a large

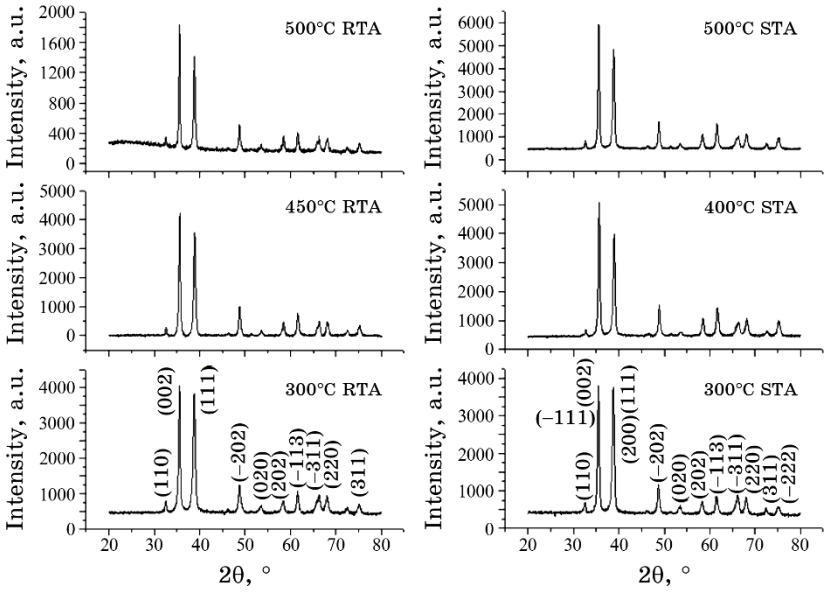

Fig. 2. XRD patterns of CuO nanoparticles prepared with RTA and STA at 300°C, 400°C, 500°C for one hour of annealing.

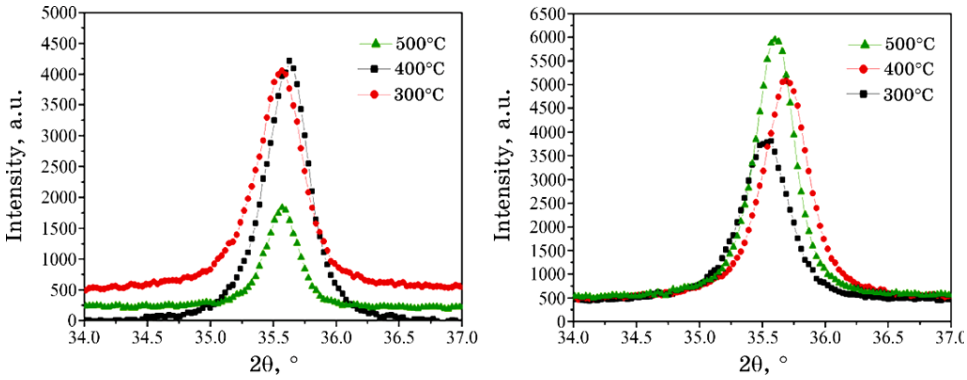

Fig. 3. The predominant peak corresponding to the (002) orientation as a function of annealing temperature and method: (*a*) RTA case; (*b*) STA case.

TABLE 1. Structural properties of CuO nanoparticles annealed following two methods.

Annealing method	STA			RTA		
Annealing temperature T, °C	300	400	500	300	400	500
Crystallite size D, nm	22.28	23.48	26.75	22.36	24.22	30.93
Strain $\varepsilon \cdot 10^{-2}$, %	0.146	0.141	0.120	0.139	0.133	0,099
Dislocation density $\delta \cdot 10^{-2}$, nm^{-2}	0.201	0.181	0.139	0,200	0.170	0.104

grain having a certain orientation. Therefore, the diffracted intensity is supposed to be increased as the crystallite size increases as in the case with STA samples. In contrast, RTA spectrum measured at 500°C revealed a significant decrease in the intensity even though the crystallite size increased at that temperature. This proves that texture may change during grain growth and affects the kinetics in the process of rapid annealing [45].

This could be justified by the fact that the rapid annealing process at high temperature (above 400°C) for one hour can favour the crystallization process, but, at the same time, may produce microcracks in the growing grains after sudden cooling from high temperature to room temperature [46, 47]. These microcracks can scatter x-rays in different directions, thereby changing the texture and reducing the peak intensity in a particular direction as indicated in Fig. 3, *a*, as it can be attributed to the grain recrystallization in contrast to recovery behaviour, which occurs in the case of RTA at relatively high temperatures [46, 47]. Recrystallization results in the formation of new grain orientations that explains the reduction of the peak intensity, and the recovery occurs during the incubation

period for recrystallization [47] that, on the other hand, explains why the grain size did not decrease. Peak intensity can increase again, when the recrystallization is completed, and this depends on both the annealing time and temperature [45–49].

For this reason, further study is required to be conducted about the effect of rapid thermal-annealing time and temperature.

The high intensity of STA peaks compared to RTA peaks may be explained by the difference in the crystal structure factor of the samples. It is known that the diffracted intensity in a particular direction is proportional to the square of the structure factor modulus. This latter reflects the total scattering from each crystal plane and depends on the distribution of atoms in the crystal structure. In other words, it is related to both the crystal structure and composition. Therefore, the peak intensity is affected by the thermal perturbation of the atoms and, more generally, by the disorder. Atoms, which have undergone rapid heating, are perturbed and susceptible to disorders more than those undergone slow heating. The latter has time to return to its equilibrium state; this leads to a low state of disorder and high diffracted intensity.

In addition, Figure 3 shows that, by increasing temperature, curves shift towards increasing θ in both methods, especially, in the STA method; this means that the nanoparticles have undergone compressive stress. This can be explained by the merging process induced by increasing thermal annealing, and this, in turn, enlarges the grain size [10, 42].

The crystalline size increases from 19.99 to 31.47 nm for temperatures from 350 to 550°C. This can be explained by the merging process induced by thermal annealing.

Table displays the calculated values of compressive stress and dislocation density (δ), where δ is determined, based on the crystallite size (D), using the formula [50]

$$\delta = D^{-2}, \tag{1}$$

whereas the microstrain values were determined using the following formula [50]:

$$\varepsilon = \frac{\beta \cos \theta}{4}. \tag{2}$$

As illustrated in Table, the dislocation density and the compressive stress values decrease as the temperature increases in both techniques of annealing. The decrease is slightly higher in RTA than in STA. The increase in the temperature stimulates the kinetics and the interactions of the dislocations. This leads to an increase in the migration and annihilation of the dislocation and, conse-

quently, to a decrease in their density.

However, rapid thermal annealing enhances the concentration of the vacancies in the lattice arrangement, which, in turn, increases the velocity of dislocation glide motion. Therefore, the dislocation density is reduced more effectively in rapid thermal annealing than in slow thermal annealing. This behaviour can also be attributed to the grain boundary effects. It is known that dislocation density, stress, and grain-boundary size are interrelated [51]. Grain boundaries contribute to the strain-hardening phenomenon in metals. They block the continued movement of dislocations in the metal during straining. As more dislocations become blocked, the metal becomes more difficult to deform. That is probably what happened in the case of the RTA, in which crystallite size takes higher values than those in STA, thereby, higher values of boundary size and lower values of stress.

3.3. Optical Analysis

The optical band-gap energy (E_g) for CuO nanoparticles was estimated employing the absorption spectrum fitting method (ASF) [52]. In this method, the optical band gap can be calculated using only the absorbance spectrum without any need for thickness. It is based on the following equation [52]:

$$A = B_1\lambda\left(\frac{1}{\lambda} - \frac{1}{\lambda_g}\right)^m + B_2, \tag{3}$$

where A is the absorbance, λ is the wavelength, B_1 and B_2 are independent on λ, m takes the value of $1/2$ for the best fitting.

Thus, the value of the band gap is obtained from $1/\lambda_g$, where E_g is equal to $1240°/\lambda_g$. The value of λ_g can be determined by extrapolating the straight line of $(A/\lambda)^2$ *versus* $1/\lambda$ curves, shown in Fig. 4, at $(A/\lambda)^2 = 0$. Table 2 displays the variation in the optical gap as a function of the annealing temperature. It can be noticed that the optical gap decreased by increasing the annealing temperature in the two cases of the annealing method.

However, the RTA method yielded lower values of the energy gap, especially, at 500°C (Fig. 5). This may be justified by the fact that the increase in particle size decreases the optical gap according to the potential-well quantum theory, *i.e.*, the quantum confinement in nanometer particle-size materials. This result confirms what is mentioned above (Fig. 1): the particle size for RTA is larger than the particle size for STA.

On the other hand, to understand better the effect of two types

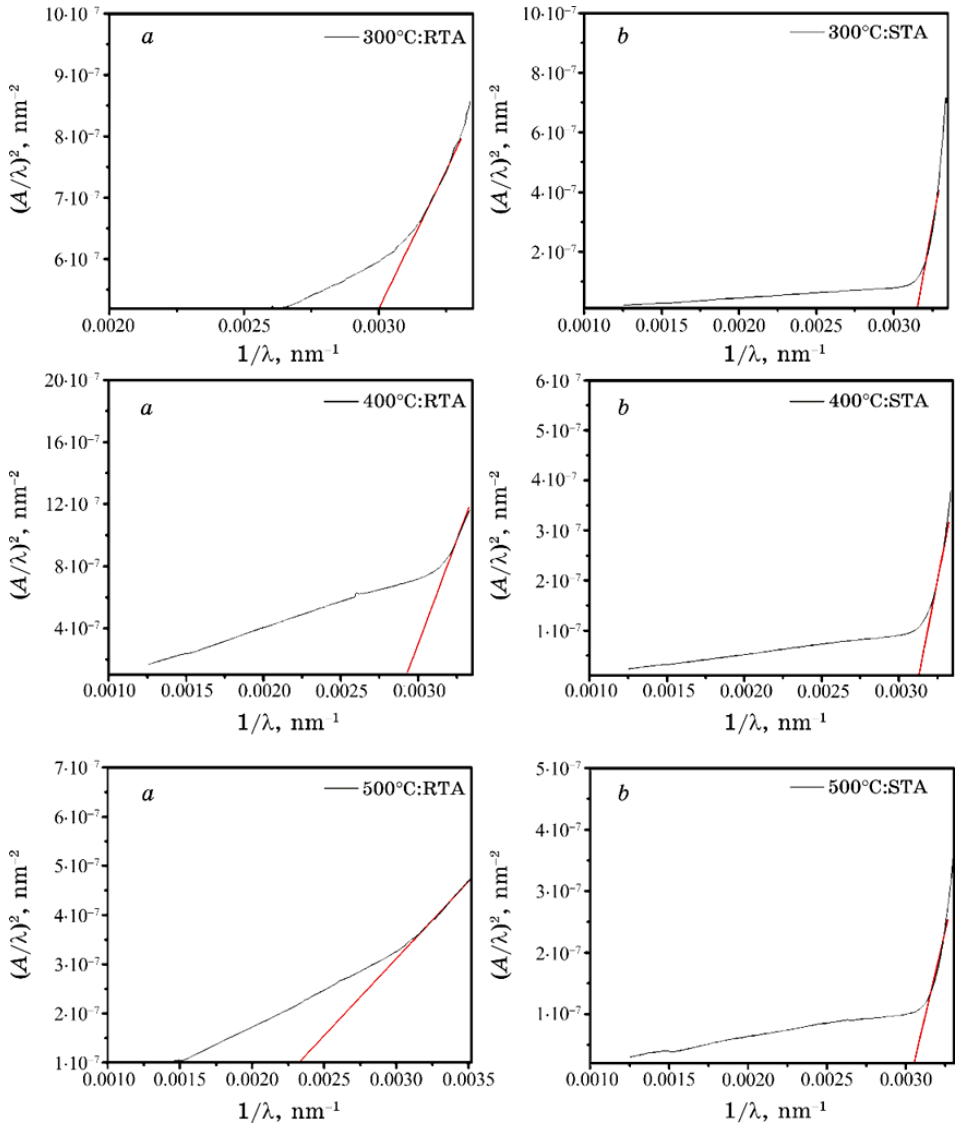

Fig. 4. ASF diagrams for samples prepared using (*a*) RTA and (*b*) STA annealing methods at 300°C, 400°C, 500°C for one hour of annealing.

of annealing processes on the structure of copper oxide, an infrared absorption bands analysis was done.

FT-IR spectra of all the samples are presented in Fig. 6. All samples' spectra show a wide band located at around 3440 cm^{-1} that corresponds to the O–H-group stretching of a water molecule adsorbed on the oxide surface [53], and an intense peak located at

TABLE 2. Energy-gap values calculated using two methods of annealing at different temperatures.

Annealing temperature T, °C	300	400	500
RTA: E_g, eV	3.72	3.63	2.88
STA: E_g, eV	3.91	3.87	3.79

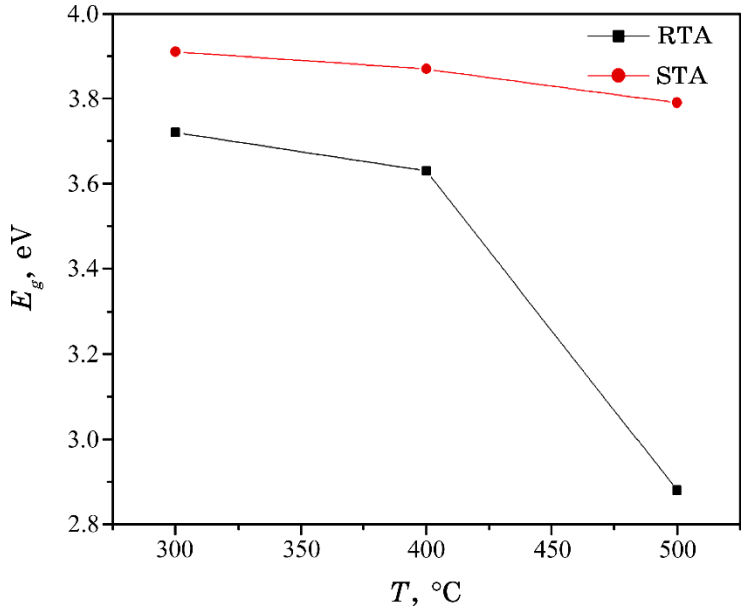

Fig. 5. Optical band-gap energy of the prepared CuO nanoparticles as a function of annealing temperature following two methods: RTA and STA for one hour of annealing.

1384 cm^{-1}, which is attributed to the stretching vibration of C=O group indicating the presence of absorbed species in the surface of nanoparticles [53, 54]. Another intense peak at around 613 cm^{-1} is attributed to the Cu–OH-vibration bands [54]; but the most intense absorption bands are located at around 494 cm^{-1} and 504 m^{-1}; it is assigned to the stretching vibrations of Cu–O indicating the formation of copper oxide [55].

It is noticed that, by increasing the annealing temperature, Cu–O-bond concentration increased and Cu–OH-bond concentration decreased, especially, in the case of RTA. However, the decrease of O–H- and C=O-bonds' concentrations is noticed in the case of STA, particularly, at 500°C, where the O–H group disappears. This means that 500°C is not sufficient to remove all residues and impurities in RTA more than in STA.

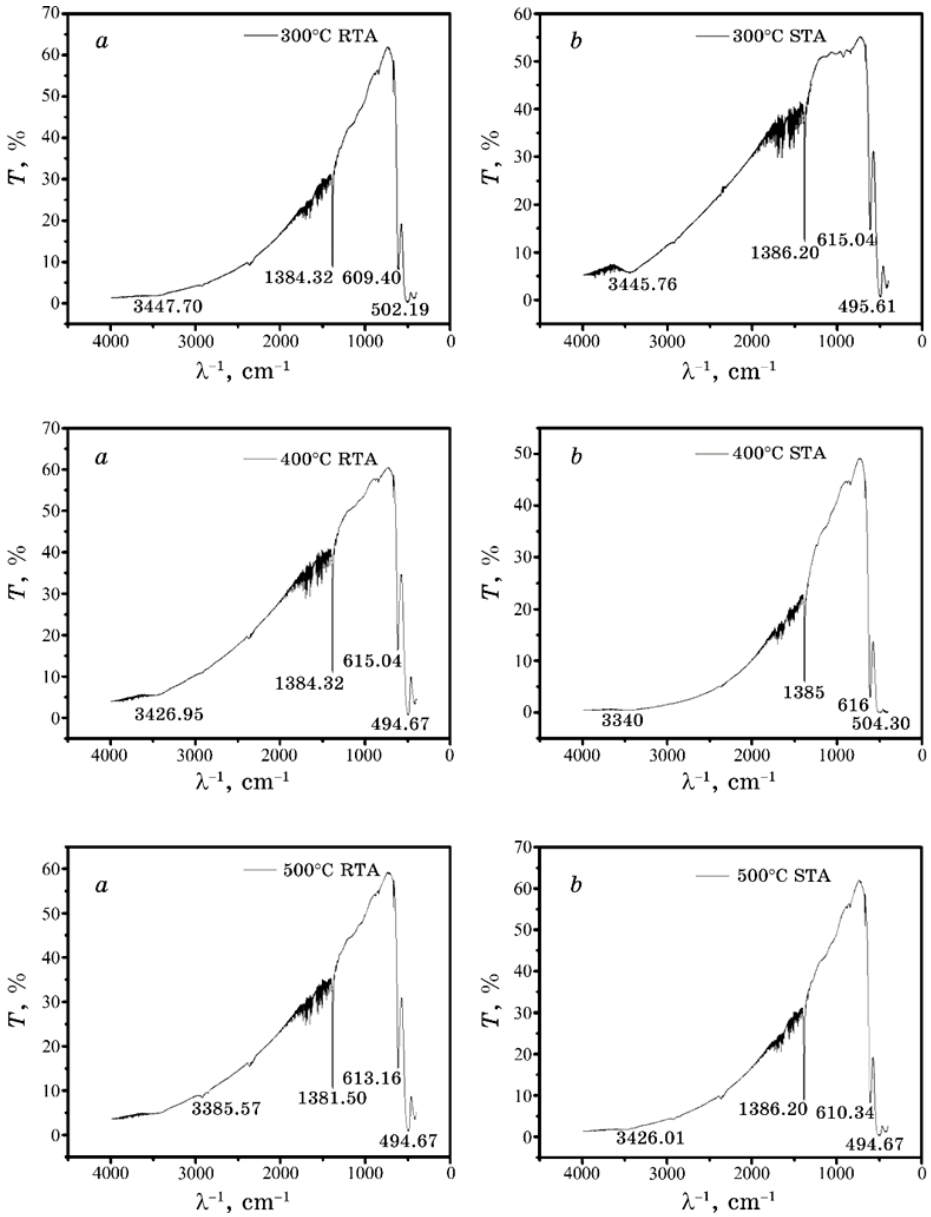

Fig. 6. FT-IR spectra of CuO nanoparticles prepared following: (*a*) RTA and (*b*) STA at 300°C, 400°C, 500°C for one hour.

No FT-IR peak of Cu_2O exists in all synthesized samples.

Both method of annealing did not affect the crystal phase of CuO nanoparticles, but affect only the crystal quality. The same result

was found in literature [41, 56].

4. CONCLUSIONS

In summary, this work reports the results of the effect of rapid and slow temperature annealing on the structural and optical properties of copper oxide nanoparticles. RTA and STA effects were studied for the first time under the same working conditions in the case of copper-oxide nanoparticles using the direct precipitation method. The objective of the work is to provide the literature with data about the effect of rapid thermal annealing on copper-oxide nanoparticles' properties and to examine the efficiency of this method of annealing compared to slow thermal annealing in enhancing CuO-nanoparticles' properties. The results showed that samples in both methods have a sheet-like shape at different tested temperatures. They reveal a change in the texture of samples, which underwent rapid thermal annealing at 500°C for 1 hour. Compared to STA, RTA at 500°C is not sufficient to remove all residues and impurities, but it has recorded relatively the lowest value of band-gap energy. Thus, rapid thermal annealing at 500°C resulted in improved optical properties of CuO nanoparticles, whereas STA resulted in improved crystalline nature of CuO nanoparticles.

We need to increase further annealing temperature and shorten the annealing time at the target temperature to study the effect of RTA on improving the crystallinity of copper-oxide nanoparticles.

REFERENCES

1. Ibrahim Khan, Khalid Saeed, and Idrees Khan, *Arabian Journal of Chemistry*, **12**, No. 7: 908 (2019); https://doi.10.1016/j.arabjc.2017.05.011
2. S. Rehman, A. Mumtaz, and S. K. Hasanain, *Journal of Nanoparticle Research*, **13**: 2497 (2011); http://dx.doi.org/10.1007/s11051-010-0143-8
3. S. Neeleshwar, C. L. Chen, C. B. Tsai, Y. Y. Chen, C. C. Chen, S. G. Shyu, and M. S. Seehra, *Physical Review B*, **71**, Iss. 20: 201307 (2005); https://doi.10.1103/PhysRevB.71.201307
4. S. Anandan, G. J. Lee, and J. J. Wu, *Ultrasonics Sonochemistry*, **19**, Iss. 3: 682 (2012); https://doi.10.1016/j.ultsonch.2011.08.009
5. Y. P. Sukhorukov, B. A. Gizhevskii, E. V. Mostovshchikova, A. Ye. Yermakov, S. N. Tugushev, and E. A. Kozlov, *Technical Physics Letters*, **32**: 132 (2006); https://doi.10.1134/S1063785006020131
6. H. Zhang and M. Zhang, *Materials Chemistry and Physics*, **108**, Iss. 2–3: 184 (2008); https://doi.org/10.1016/j.matchemphys.2007.10005
7. H. S. Devi and T. D. Singh, *Advances in Electronics and Electrical Engineering*, **4**, Iss. 1: 83 (2014).
8. J. Zhu, D. Li, H. Chen, X. Yang, L. Lu, and X. Wang, *Materials Letters*, **58**, Iss. 26: 3324 (2004); https://doi.org/10.1016/j.matlet.2004.06.031

9. P. Mallick and S. Sahu, *Nanoscience and Nanotechnology*, **2**, Iss. 3: 71 (2012); https://doi.org/10.5923/j.nn.20120203.05
10. N. Touka, D. Tabli, K. Badari et al., *Journal of Optoelectronics and Advanced Materials*, **21**, Iss. 12: 698 (2019).
11. N. A. Raship, M. Z. Sahdan, F. Adriyanto, M. F. Nurfazliana, and A. S. Bakri, *AIP Conference Proceedings*, **1788**, Iss. 1: 030121 (2017); https://doi.org/10.1063/1.4968374
12. N. Serin, T. Serin, Ş. Horzum, and Y. Çelik, *Semiconductor Science and Technology*, **20**, Iss. 5: 398 (2005); https://doi.org/10.1088/02681242/20/5/012
13. S. Masudy-Panah, R. S. Moakhar, C. S. Chua, A. Kushwaha, T. I. Wong, and G. K. Dalapati, *RSC Advances*, **6**, Iss. 35: 29383 (2016); https://doi.org/10.1039/C6RA03383K
14. R. Gottesman, A. Song, I. Levine, M. Krause, A. N. Islam, D. Abou-Ras, T. Dittrich, R. van de Krol, and A. Chemseddine, *Advanced Functional Materials*, **30**, Iss. 21: 1910832 (2020); https://doi.org/10.1002/adfm.201910832
15. K. Bergum, H. N. Riise, S. Gorantla, P. F. Lindberg, I. J. T. Jensen, A. E. Gunnæs, A. Galeckas, S. Diplas, B. G. Svensson, and E. Monakhov, *Journal of Physics: Condensed Matter*, **30**, Iss. 7: 075702 (2018); doi:10.1088/1361-648X/aaa5f4
16. R. B. Vasiliev, M. N. Rumyantseva, N. V. Yakovlev, and A. M. Gaskov, *Sensors and Actuators B: Chemical*, **50**, Iss. 3: 186 (1998); https://doi.10.1016/S0925-4005(98)00235-4
17. T. Ishihara, M. Higuchi, T. Takagi, M. Ito, H. Nishiguchi, and Y. Takita, *Journal of Materials Chemistry*, **8**, Iss. 9: 2037 (1998); https://doi.10.1039/A801595C
18. Sylvester Lekoo Mammah, Fidelix Ekeoma Opara, Valentine Benjamin Omubo-Pepple, Joseph Effiom-Edem Ntibi, Sabastine Chukwuemeka Ezugwu, and Fabian Ifeanyichukwu Ezema, *Natural Science*, **5**, Iss. 3: 389 (2013); https://doi.10.4236/ns.2013.53052
19. H. Hashim, S. F. A. Samat, S. S. Shariffudin, and P. S. M. Saad, *IOP Conference Series: Materials Science and Engineering*, **340**, Iss. 1: 012008 (2018); https://doi.10.1088/1757899X/340/1/012008
20. D. Wojcieszak, A. Obstarczyk, E. Mańkowska, M. Mazur, D. Kaczmarek, K. Zakrzewska, P. Mazur, and J. Domaradzki, *Materials Research Bulletin*, **147**: 111646 (2022); https://doi.10.1016/j.materresbull.2021.111646
21. N. Al Armouzi, Gh. El Hallani, A. Liba, M. Zekraoui, H. S. Hilal, N. Kouider, and M. Mabrouki, *Materials Research Express*, **6**, Iss. 11: 116405 (2019); https://doi.10.1088/2053-1591/ab44f3
22. U. Akgul, K. Yildiz, and Y. Atici, *The European Physical Journal Plus*, **131**, Iss. 89: 1 (2016); doi:10.1140/epjp/i2016160893
23. G. Martínez-Saucedo, G. Torres-Delgado, J. Márquez-Marín, O. Zelaya-Ángel, and R. Castanedo-Pérez, *Journal of Alloys and Compounds*, **859**: 157790 (2021); doi:101016/jjallcom2020157790
24. L. Xiong, H. Xiao, S. Chen, Z. Chen, X. Yi, S. Wen, G. Zheng, Y. Ding, and H. Yu, *RSC Advances*, **4**, Iss. 107: 62115 (2014); https://doi.org/10.1039/C4RA12406E
25. Dongjing Liu, Weiguo Zhou, and Jiang Wu, *The Canadian Journal of*

Chemical Engineering, **94**, Iss. 12: 2276 (2016); https://doi.org/10.1002/cjce.22613
26. A. Maini and M. A. Shah, *International Journal of Ceramic Engineering & Science*, **3**, Iss. 4: 192 (2021); https://doi.org/10.1002/ces210097
27. M. B. Gawande, A. Goswami, F. X. Felpin, T. Asefa, X. Huang, R. Silva, X. Zou, R. Zboril, and R. S. Varma, *Chemical Reviews*, **116**, Iss. 6: 3722 (2016); https://doi.org/10.1021/acs.chemrev5b00482
28. Dongjing Liu, Weiguo Zhou, and Jiang Wu, *The Canadian Journal of Chemical Engineering*, **94**, Iss. 12: 2276 (2016); https://doi.org/10.1002/cjce.22613
29. G. Eranna, B. C. Joshi, D. P. Runthala, and R. P. Gupta, *Critical Reviews in Solid State and Materials Sciences*, **29**, Iss. 3–4: 111 (2004); https://doi.org/10.1080/10408430490888977
30. P. Gao, Y. Chen, H. Lv, X. Li, Y. Wang, and Q. Zhang, *International Journal of Hydrogen Energy*, **34**, Iss. 7: 3065 (2009); https://doi.org/10.1016/j.ijhydene200812.050
31. T. I. Arbuzova, B. A. Gizhevskii, S. V. Naumov, A. V. Korolev, V. L. Arbuzov, K. V. Shal'nov, and A. P. Druzhkov, *Journal of Magnetism and Magnetic Materials*, **258**: 342 (2003); https://doi.org/10.1016/S0304-8853(02)01052-1
32. X. P. Gao, J. L. Bao, G. L. Pan, H. Y. Zhu, P. X. Huang, F. Wu, and D. Y. Song, *The Journal of Physical Chemistry B*, **108**, Iss. 18: 5547 (2004); https://doi.org/10.1021/jp037075k
33. P. P. C. Udani, P. V. D. S. Gunawardana, H. C. Lee, and D. H. Kim, *International Journal of Hydrogen Energy*, **34**, Iss. 18: 7648 (2009); https://doi.org/10.1016/j.ijhydene.2009.07035
34. A. Toolabia, M. R. Zareb, A. Rahmanic, E. Hoseinzadehd, M. Sarkhoshe, and M. Zaref, *J. Basic. Appl. Sci. Res.*, **3**, Iss. 2: 221 (2013).
35. S. Jadhav, S. Gaikwad, M. Nimse, and A. Rajbhoj, *Journal of Cluster Science*, **22**: 121 (2011); https://doi.org/101007/s1087601103497
36. A. Rahim, Z. U. Rehman, S. Mir, N. Muhammad, F. Rehman, M. H. Nawaz, M. Yaqub, S. A. Siddiqi, and A. A. Chaudhry, *Journal of Molecular Liquids*, **248**: 425 (2017); https://doi.org/10.1016/j.molliq 2017.10.087
37. D. Rehana, D. Mahendiran, R. S. Kumar, and A. K. Rahima, *Biomedicine & Pharmacotherapy*, **89**: 1067 (2017); https://doi.org/10.1016/j.biopha2017.02.101
38. Sunday Adewale Akintelu, Aderonke Similoluwa Folorunso, Femi Adekunle Folorunso, and Abel Kolawole Oyebamiji, *Heliyon*, **6**, Iss. 7: e04508 (2020); doi:10.1016/j.heliyon.2020.e04508
39. Y. Unutulmazsoy, C. Cancellieri, L. Lin, and L. P. H. Jeurgens, *Applied Surface Science*, **588**: 152896 (2022); https://doi.org/10.1016/j.apsusc.2022.152896
40. T. T. Ha, B. T. Cong, P. N. Hai, N. Hoang, H. V. Chinh, B. T. Huong, N. T. Linh, B. T. Son, T. T. Q. Hoa, and T. N. Viet, *VNU Journal of Science: Mathematics-Physics*, **38**, Iss. 2: 4642 (2022); doi:10.25073/2588-1124/vnumap4642
41. V. U. Siddiqui, A. Ansari, I. Khan, M. K. Akram, and W. A. Siddiqi, *Materials Research Express*, **6**, Iss. 11: 115095 (2019); doi:10.1088/2053-1591/ab4ace

42. S. N. Khan, S. Ge, E. Gu, S. K. Karunakaran, W. Yang, R. Hong, Y. Mai, X. Lin, and G. Yang, *Advanced Materials Interfaces*, **8**, Iss. 18: 2100971 (2021); doi:10.1002/admi.202100971
43. Roland Mainz, B. C. Walker, S. S. Schmidt, O. Zander, A. Weber, H. Rodriguez-Alvarez, J. Just, M. Klaus, R. Agrawal, and T. Unold, *Physical Chemistry Chemical Physics*, **15**, Iss. 41: 18281 (2013); https://doi.org/10.1039/C3CP53373E
44. A. A. Baqer, K. A. Matori, N. M. Al-Hada, A. H. Shaari, H. M. Kamari, E. Saion, J. L. Y. Chyi, and C. Azurahanim Abdullah, *Results in Physics*, **9**: 471 (2018); https://doi.101016/j.rinp2018.02.079
45. A. Rollett, F. J. Humphreys, G. S. Rohrer, and G. H. Hatherly, *Recrystallization and Related Annealing Phenomena* (Burlington: Elsevier Science: 2004), 658 p.
46, Y. C. Lee, S. Y. Hu, W. Water, K. K. Tiong, Z. C. Feng, Y. T. Chen, J. C. Huang, J. W. Lee, C. C. Huang, J. L. Shen, and Mou-Hong Cheng, *Journal of Luminescence*, **129**, Iss. 2: 148 (2009); doi:10.1016/j.jlumin.2008.09.003
47. M. K. Puchert, P. Y. Timbrell, and R. N. Lamb, *Journal of Vacuum Science & Technology A: Vacuum, Surfaces, and Films*, **14**, Iss. 4: 2220 (1996); doi:10.1116/1580050
48. P. Cotterill and P. R. Mould, *Recrystallization and Grain Growth in Metals* (London: Surrey Univ. Press: 1976), 409 p.
49. P. R. Rios, F. Siciliano Jr., H. R. Z. Sandim, R. L. Plaut, and A. F. Padilha, *Materials Research*, **8**: 225 (2005); doi:10.1590/S1516-14392005000300002
50. L. Zhou, S. Wang, H. Ma, S. Ma, D. Xu, and Y. Guo, *Chemical Engineering Research and Design*, **98**: 36 (2015); doi:10.1016/j.cherd.2015.04.004
51. D. Z. Voyiadjis, D. Faghihi, and Y. Zhang, *International Journal of Solids and Structures*, **51**, Iss. 10: 1872 (2014); doi:10.1016/j.ijsolstr.2014.01.020
52. N. Ghobadi, *International Nano Letters*, **3**, Iss. 1: 2 (2013); https://doi.10.1186/2228-5326-3-2
53. J. M. Aguirre, A. Gutiérrez, and O. Giraldo, *Journal of the Brazilian Chemical Society*, **22**: 546 (2011); doi:10.1590/S0103-50532011000300019
54. C. Henrist, K. Traina, C. Hubert, G. Toussaint, A. Rulmont, and R. Cloots, *Journal of Crystal Growth*, **254**, Iss. 1–2: 176 (2003); doi:10.1016/S0022-0248(03)01145-X
55. J. Liu, X. Huang, Y. Li, K. M. Sulieman, X. He, and F. Sun, *Journal of Materials Chemistry*, **16**, Iss. 45: 4427 (2006); https://doi.10.1039/C6DT04500
56. F. A. Akgul, G. Akgul, N. Yildirim, H. E. Unalan, and R. Turan, *Materials Chemistry and Physics*, **147**, Iss. 3: 987 (2014); doi:10.1016/j.matchemphys 2014.06.047